Crack Nucleation and Branching in the eXtended Finite Element Method

by

Mark Merewether

Department of Civil and Environmental Engineering
Duke University

Date: _____

Approved:

_____
John Dolbow, Supervisor

_____
Wilkins Aquino

_____
Guglielmo Scovazzi

Thesis submitted in partial fulfillment of the requirements for the degree of
Master of Science in the Department of Civil and Environmental Engineering
in the Graduate School of Duke University
2013

Abstract

Crack Nucleation and Branching in the eXtended Finite Element Method

by

Mark Merewether

Department of Civil and Environmental Engineering
Duke University

Date: _____

Approved:

_____
John Dolbow, Supervisor

_____
Wilkins Aquino

_____
Guglielmo Scovazzi

An abstract of a thesis submitted in partial fulfillment of the requirements for the degree of Master of Science in the Department of Civil and Environmental Engineering in the Graduate School of Duke University
2013

Abstract

The eXtended Finite Element Method (X-FEM) has proven to be a robust method for simulating crack propagation, but relatively little work has focused on the important problem of crack initiation or nucleation. In this work, we examine various options for nucleating cracks within a cohesive framework and the X-FEM. Attention is confined to shell problems. We discuss the details of the methods and their strengths and weaknesses. With the introduction of such nucleation algorithms, the need to model more complex crack growth topologies also arises. In particular, we examine algorithms for enabling crack branching, focusing on both the mechanics and element kinematic considerations. The results of various benchmark problems for the nucleation and branching algorithms are also presented and discussed.

Contents

List of Figures

Acknowledgements

I would first like to thank my parents for the strong upbringing: for instilling in me the desire to work hard and have a positive impact on society. I would like to thank Sandia National Laboratories, and my manager Joe Jung, for sponsoring my research as well as my graduate education. I greatly look forward to continuing the work we have accomplished, striving to perform exceptional service in the national interest. I would like to thank my advisor John Dolbow for sharing his knowledge of engineering with me, and for all of his efforts in helping me achieve my degree. I also have a great amount of gratitude for Andy Stershic: for his significant contributions to this project and for his friendship. I would also like to thank all of my labmates in the DCML: Ziyu Zhang, Wen Jiang, Chandrasekhar Annavarapu, Anand Embar, Temesgen Kindo, Curtis Lee, Alex Kelly, Yan Feng, and Bingxiao Zhao. Most of all, I thank God for allowing me to have this great opportunity, for giving me the skills necessary to complete this program, and for providing me with this great life that I have.

1

Introduction

The methods of modeling fracture in computational mechanics have had vast improvements in accuracy and efficiency over the last twenty years. The eXtended Finite Element Method (X-FEM) offered great promise in these areas with its robust means of element cutting and no requirement of remeshing the geometry to generate acceptable results. The X-FEM also created the ability to efficiently simulate complex geometries [2], thus expanding the scope of solvable fracture problems. It is these reasons that have motivated many to pursue the X-FEM over other various fracture modeling methods.

In past implementations of the X-FEM, crack growth could be modeled accurately, but the need to model crack generation (or nucleation) remained. This study proposes three methods of crack nucleation in the X-FEM: element-based nucleation, edge-based nucleation, and one-ring-based nucleation. The nucleation capabilities implemented examine the stress concentration (or another user defined element variable) of each element and determine when to nucleate a crack based on these calculations.

Intuitively, because many crack nucleation problems involve large deformation and/or contact, single cracks must have the ability to develop into multiple cracks or merge with existing cracks. A crack branching capability was created in order to account for these various crack modes. The crack branching capability examines the stress concentration (or another user defined element variable) of the already failed elements and determines when a crack should branch.

The overall goal is to successfully predict fracture in an un-fractured geometry and to correctly follow the speed, direction, and branching of the existing crack(s) if necessary. The benchmarking problems put forth in this paper are either physical

problems where the result is known, problems that have been modeled by other fracture modeling capabilities (such as the cohesive network approach, element death, MLEP Fail, etc.), or slight variants of problems previously solved by the X-FEM with no nucleation or branching.

2

Problem Formulation and Governing Equations

In this section, we will briefly outline the problem formulation as well as the associated governing equations of elastodynamics. We will also briefly outline how the shell element formulations are applied after the general derivation.

2.1 Governing Equations

Consider the domain Ω bounded by Γ (Figure 2.1). The strong form of the equilibrium equations is given by:

$$
\begin{aligned}
-\rho\ddot{u}_i + \sigma_{ij,j} + b_i = 0 \qquad & in\ \Omega \\
u_i = g_i \qquad & on\ \Gamma_{gi} \\
\sigma_{ij} n_j = h_i \qquad & on\ \Gamma_{hi}
\end{aligned}
$$

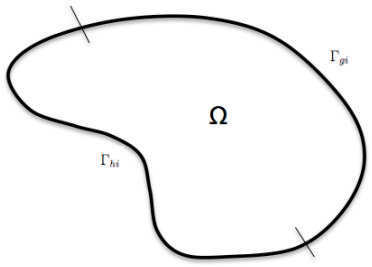

FIGURE 2.1: Body with associated boundary conditions.

where ρ is the density, u_i is the displacement vector, σ_{ij} is the cauchy stress tensor, b_i is the body force vector, and n_j is the unit outward normal. After multi-

plying by the virtual displacement vector v_i and integrating by parts, we obtain the equation in the form:

$$\int_\Omega \rho \ddot{u}_i v_i \, d\Omega + \int_\Omega \sigma_{ij} v_{i,j} \, d\Omega = \int_\Omega b_i v_i \, d\Omega + \int_{\Gamma_{h_i}} h_i v_i d\Gamma$$

After obtaining this form, we can manipulate the equation to produce the weak form. Given b, g, h, u_0, and $\dot{u_0}$, find $u(t)$, such that for all $v \in \mathcal{V}$,

$$(v,\ \rho\ddot{u}) \ +\ a(v,\ u) \ =\ (v,\ b) \ +\ (v,\ h)_\Gamma$$

$$(v,\ \rho u(0)) \ =\ (v,\ \rho u_0)$$

$$(v,\ \rho\dot{u}(0)) = (v,\ \rho\dot{u}_0)$$

Once we obtain the weak form, we can rearrange the equation to form the matrix problem

$$M\ddot{d} \ +\ Kd \ =\ F$$

$$d(0) = d_0$$

$$\dot{d}(0) = \dot{d}_0$$

by discretizing the weak form. To this point, the derivation is the same no matter which element type is used during the simulation. After transforming the global mass matrix and stiffness matrix into the local element domain, they can be given as:

$$m^e \ =\ \delta_{ij} \int_{\Omega_e} N_a \rho N_b \, d\Omega$$

$$k^e \ =\ e_i^T \int_{\Omega_e} B_a^T D B_b \, d\Omega \, e_j$$

The B and D matrices are formulated with the various element formulation and material property parameters. Special care must be taken in formulating these matrices because they now compose of both translational and rotational components (as well as any hourglass-control mechanisms the shell element formulation requires). The force vector is also comprised of both translational and rotational components and formed using a combination of the element shape functions, external force vectors, and boundary conditions (varies, depending on the element formulation that is chosen). The shell element formulation used in all simulations was that proposed by Ted Belytschko, Jerry Lin, and Chen-Shyh Tsay. Briefly, the velocity-strain relationships for the element are given by

$$\hat{d}_x = \frac{\partial \hat{v}_x^m}{\partial \hat{x}} + \hat{z}\frac{\partial \hat{\theta}_y}{\partial \hat{x}} \qquad \hat{d}_y = \frac{\partial \hat{v}_y^m}{\partial \hat{y}} - \hat{z}\frac{\partial \hat{\theta}_x}{\partial \hat{y}}$$

$$2\hat{d}_{xy} = \frac{\partial \hat{v}_x^m}{\partial \hat{y}} + \frac{\partial \hat{v}_y^m}{\partial \hat{z}} + \hat{z}\left(\frac{\partial \hat{\theta}_y}{\partial \hat{y}} - \frac{\partial \hat{\theta}_x}{\partial \hat{x}}\right) \qquad 2\hat{d}_{yz} = \frac{\partial \hat{v}_z^m}{\partial \hat{y}} - \hat{\theta}_x \qquad 2\hat{d}_{xz} = \frac{\partial \hat{v}_z^m}{\partial \hat{x}} - \hat{\theta}_y$$

and the internal force vectors are given by

$$\hat{f}_{xi} = A(B_{1I}\mathcal{F}_x + B_{2I}\mathcal{F}_{xy}) \qquad \hat{f}_{yi} = A(B_{2I}\mathcal{F}_y + B_{1I}\mathcal{F}_{xy}) \qquad \hat{f}_{zi} = A\bar{\kappa}(B_{1I}\mathcal{F}_{xz} + B_{2I}\mathcal{F}_{yz})$$

$$\hat{m}_{xi} = A[B_{2I}\mathcal{M}_y + B_{1I}\mathcal{M}_{xy} - \frac{1}{4}\bar{\kappa}\mathcal{F}_{yz}] \qquad \hat{m}_{yi} = A[-B_{1I}\mathcal{M}_x + B_{2I}\mathcal{M}_{xy} + \frac{1}{4}\bar{\kappa}\mathcal{F}_{xz}] \qquad \hat{m}_{zi} = 0$$

where A is the element area, B is composed of the four element shape functions with two components, $\bar{\kappa}$ is the shear factor, and

$$\mathcal{F}_{\alpha\beta} = \int \hat{\sigma}_{\alpha\beta}\, d\hat{z} \qquad \mathcal{M}_{\alpha\beta} = -\int \hat{z}\hat{\sigma}_{\alpha\beta}\, d\hat{z}$$

Further information can be found in Belytschko et al. (2006). For the eXtended Finite Element Method, once the weak form of the equations are found, approximations need to be configured in order to predict discontinuities across a crack. In

order for these to be accurately calculated, node enrichment is performed on nodes that contain a crack front. As presented in Moes et al. (1999), the displacement approximation prior to the discontinuity is:

$$u^h = \sum_{i \in D} u_i \phi_i$$

and after the discontinuity is:

$$u^h = \sum_{i \in D} u_i \phi_i + \sum_{j \in D\prime} b_j \phi_j H(x)$$

where D is the set of all degrees of freedom, D' is the set of nodes whose support overlaps the crack geometry, H(x) is known as the Heaviside jump (or step) function, and the ϕ functions are the bilinear shape functions associated with the corresponding nodes. Further details of numerical integration and implementation can be found within the paper.

The shell cohesive model that was used for the shell simulations was the Alves-Roehl cohesive model Alves and Roehl (2012). The Alves-Roehl cohesive model is a Xu-Needleman like cohesive model that includes a rotational component to account for the crack growth through the thickness of the shell element. The shape of the cohesive model is given by:

$$\phi = \phi_n\{1 - (1 + \frac{\Delta_n}{\delta_n})exp(-\frac{\Delta_n}{\delta_n})exp(-\frac{\Delta_t^2}{\delta_t^2})exp(-\frac{\Delta_\theta^2}{\delta_\theta^2})\}$$

and from the shape, the traction is given by:

$$t_c = \frac{\partial \phi}{\partial \Delta}$$

After differentiating with respect to each component, we have the governing equations of the cohesive zone below.

$$T_n = \frac{\partial \phi}{\partial \Delta_n} = \frac{\phi_n \Delta_n}{\delta_n^2} exp(-\frac{\Delta_n}{\delta_n}) exp(-\frac{\Delta_t^2}{\delta_t^2}) exp(-\frac{\Delta_\theta^2}{\delta_\theta^2})$$

$$T_{ti} = \frac{\partial \phi}{\partial \Delta_{ti}} = \frac{2\phi_{ti} \Delta_{ti}}{\delta_{ti}^2} (1 + \frac{\Delta_n}{\delta_n}) exp(-\frac{\Delta_n}{\delta_n}) exp(-\frac{\Delta_t^2}{\delta_t^2}) exp(-\frac{\Delta_\theta^2}{\delta_\theta^2})$$

$$M_\theta = \frac{\partial \phi}{\partial \Delta_\theta} = \frac{2\phi_\theta \Delta_\theta}{\delta_\theta^2} (1 + \frac{\Delta_n}{\delta_n}) exp(-\frac{\Delta_n}{\delta_n}) exp(-\frac{\Delta_t^2}{\delta_t^2}) exp(-\frac{\Delta_\theta^2}{\delta_\theta^2})$$

3

Previously Existing X-FEM Capabilities

In this section, we will outline the previously existing X-FEM framework in which we did our development. First, we will briefly describe the duplication algorithm proposed by Richardson et al. (2011), then we will move into the specifics of the existing cutting methods.

3.1 The Duplication Algorithm

The duplication algorithm has already gained great prowess in the field of graphics and computer simulation, but has had little exposure to the world of finite elements thus far. In this paper, we attempt to bridge the gap between the two, potentially resulting in fracture solutions that have not been seen before in the finite element community.

The duplication algorithm is based on the concept of duplicating all mesh parts of an element (nodes, faces, and the element itself). This is done through the bookkeeping of parent IDs (the original element components) and child IDs (the duplicated element components). After the mesh parts are duplicated geometrically, the field data is passed on from the parent to the children (displacement fields, energy fields, etc.). The new child mesh parts are given their own global ID numbers and become part of the mesh. When an element is cut with the X-FEM, that element is split into two child elements.

3.2 The Cutting Mechanisms

The mechanisms that were previously developed for cutting elements included cutting a single element by cutting it's edges or cutting multiple elements by prescribing a

failure plane. For the failure plane, a midpoint of the plane was required input, as well as a radius of the plane and a rotational orientation vector. After a crack formed in the geometry by the failure plane, the crack was allowed to grow by either planar growth or piecewise-linear growth. Crack growth occurs when the user defined element variable is reached (usually some sort of stress) by an element in front of the crack tip. If piecewise-linear growth is chosen, the direction of the crack is determined by calculating the stress eigenvectors within the element, and taking the normal of this calculation.

4

The Nucleation Capabilities

In this section, we describe the three nucleation capabilities implemented and briefly describe the differences between them and the impact on the results. For all nucleation methods, a restriction is imposed that does not allow nucleation to occur on elements directly surrounding the elements previously failed by nucleation. This was done in order to encourage those elements to fail by mechanics growth of the nearby crack (because it is much easier for a crack to grow than for a separate crack to form nearby).

4.1 Element-Based Nucleation

Element-based nucleation involves cutting a single element if it exceeds the failure criterion. The user-defined failure condition is examined for each element, and if the value becomes greater than the failure criteria, the element is cut. The crack is formed by the insertion of a failure plane at the midpoint of the element and at an angle calculated using the stress eigenvectors of the element. The length of the failure plane is slightly larger than the length of the element but not extending into any other elements, making this element's failure complete without failing adjacent elements.

As expected, problems simulated using element-based nucleation have generated cracks sooner and more frequently than the other two methods. Because of this, as well as the coupled crack growth and branching capabilities, the dynamics of the problem can possibly be significantly affected.

4.2 Edge-Based Nucleation

Edge-based nucleation is based on cutting individual edges shared by two elements. The user-defined failure condition is examined for each element, and if the value becomes greater than the failure criteria, the element is stored. Then, the elements surrounding the stored element are examined, and if any of them have reached the failure criteria, a crack is allowed to nucleate across the edge shared by the two elements. To form the crack, a cut-plane is inserted at the midpoint of the edge and at an angle calculated using the stress eigenvectors of the two elements. The length of the plane is calculated using the length of the two elements, and scaled by a value only allowing the two elements to be cut.

Edge-based nucleation has produced excellent results for many problem sets, but there are some problems that have shown issues with the method. Because the method cuts the edge of two adjacent elements, sometimes the crack is shifted from the actual physical location. A problem displaying this issue is presented in Section 5.1.

4.3 One-Ring-Based Nucleation

A one-ring is a set of elements that are all connected by a single node. The various forms of a one-ring for quadrilateral elements can be seen in Figure 4.1. For one-ring based nucleation, a crack is only allowed to form when all of the elements in a one-ring have reached the failure criterion.

Once all of the elements within the one-ring reach the failure criterion, a failure plane slightly larger than the length of the one-ring group of elements is inserted on the fly. The plane is inserted at the midpoint of the one-ring and at an angle calculated using the stress eigenvectors of the elements within the one-ring.

Naturally, a more refined mesh may be required to accurately solve certain prob-

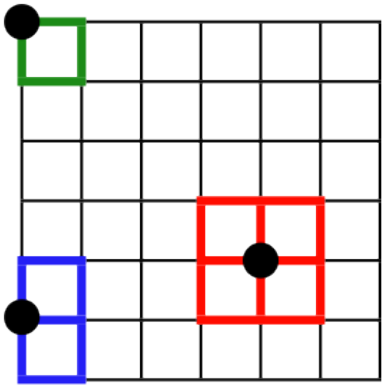

FIGURE 4.1: Demonstration of quadrilateral shell element one-rings.

lems using this algorithm. However, this algorithm has proven to be more accurate than the other methods for certain problems.

5

Numerical Examples for Nucleation

The purpose of the following numerical examples is to evaluate the implemented nucleation methods. The problems solved have a known solution (either experimentally or computationally), and have some measure of comparison with other documented results. The following numerical examples were run using the Sierra Mechanics finite element software produced by Sandia National Laboratories, using explicit dynamics. All of the problems were solved using the Belytschko-Tsay shell element [Belytschko et al. (2006)] with an hourglass stiffness value of 0.8 and an hourglass viscosity value of 0.2. The material properties that were used for every simulation can be found in Appendix 1. Unless otherwise specified, the criterion used to initiate nucleation, propagation, or branching was always the maximum principal stress.

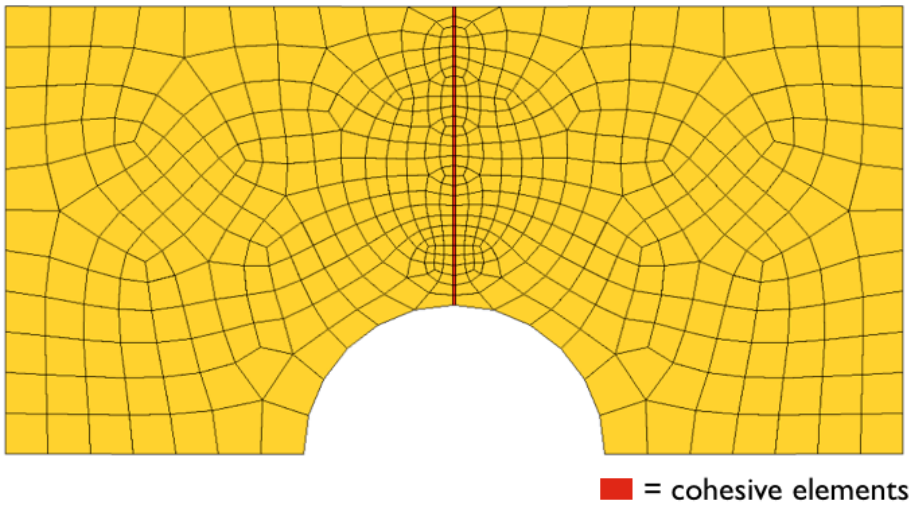

FIGURE 5.1: Cohesive elements insertion.

The result that were used to compare the X-FEM results to were generated by manually embedding cohesive elements along the expected crack path (Figure 5.1- a further explanation of cohesive elements can be found in Section 7.1). Because the

X-FEM crack growth is limited to planar growth, this is a reasonable comparison to make. When the input value of cohesive energy is reached, the cohesive zone gives way and a "crack" is formed.

5.1 Plate with a hole under tensile loading

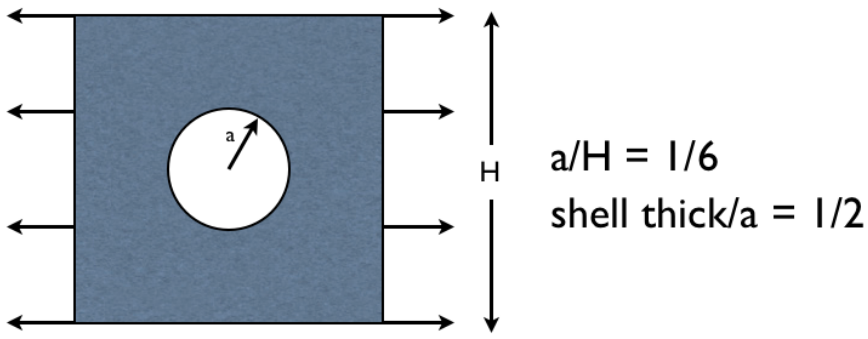

FIGURE 5.2: Plate with hole problem setup.

Consider the problem shown in Figure 5.2: a plate with a hole under uniform tensile loading. As the force increases as the sides are pulled apart, a stress concentration forms at the top and bottom of the hole. Once the stress concentration reaches the fracture stress, a crack nucleates at this location.

A comparative study was done for this problem, comparing the results found using cohesive elements inserted at the crack location and the results found using the new X-FEM nucleation methods and cohesive zones inserted after the X-FEM crack is generated. The shell cohesive model that was used for the comparison was the Alves-Roehl model. For comparative simplicity, only half of the plate was modeled, the crack was only allowed to grow in a planar fashion, and nucleation was only allowed to occur once during the simulation. Force-displacement curves were generated and

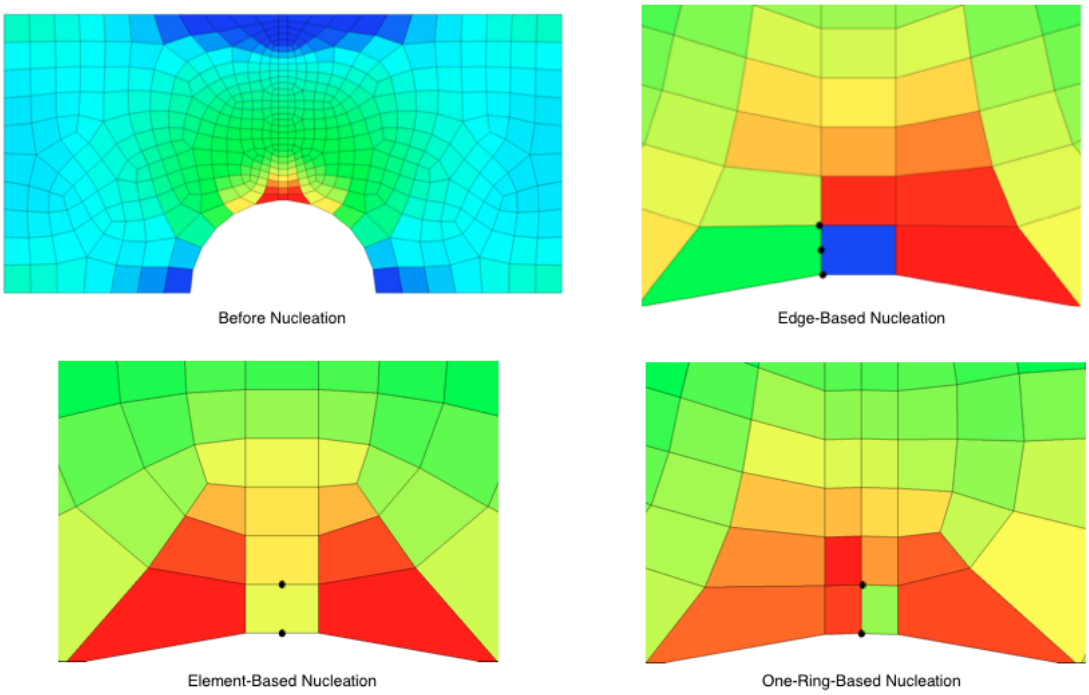

FIGURE 5.3: Plate with hole nucleation results.

the results are compared.

The X-FEM nucleation capabilities that performed the best for this problem were the element-based nucleation and the one-ring-based nucleation. For the edge-based nucleation, it is apparent that the two elements that reached the failure criterion were both along the curved edge of the geometry. Therefore, a crack was inserted at the midpoint of the edge joining these two elements, resulting in a crack that is shifted to one side instead of through the center of the middle element (Figure 5.3). Thus, we recommend using the element-based nucleation or one-ring-based nucleation when solving fracture problems involving holes.

As can be seen from the graphs below (Figure 5.4 and 5.5), the element based nucleation and the one-ring based nucleation methods generate results very close to the cohesive zone results. Crack nucleation occurs at almost exactly the same force for the three techniques and at the same location within the mesh. The slight

variation in displacement is likely due to slight differences in the meshes.

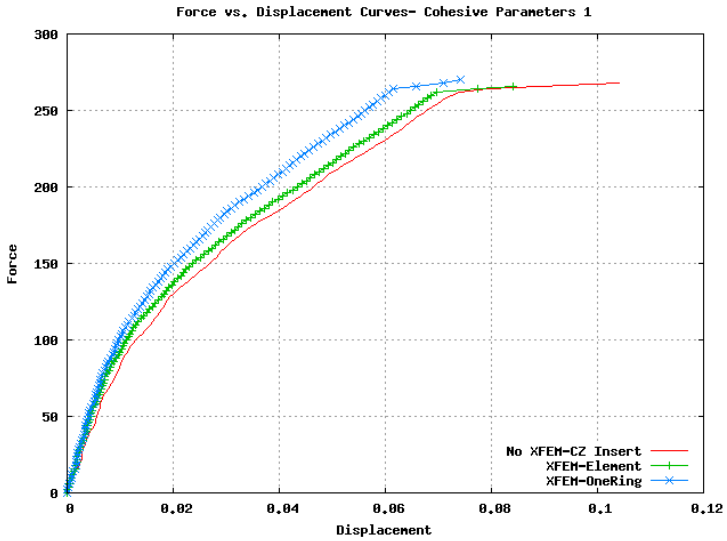

FIGURE 5.4: Force vs. displacement curve for cohesive parameters.

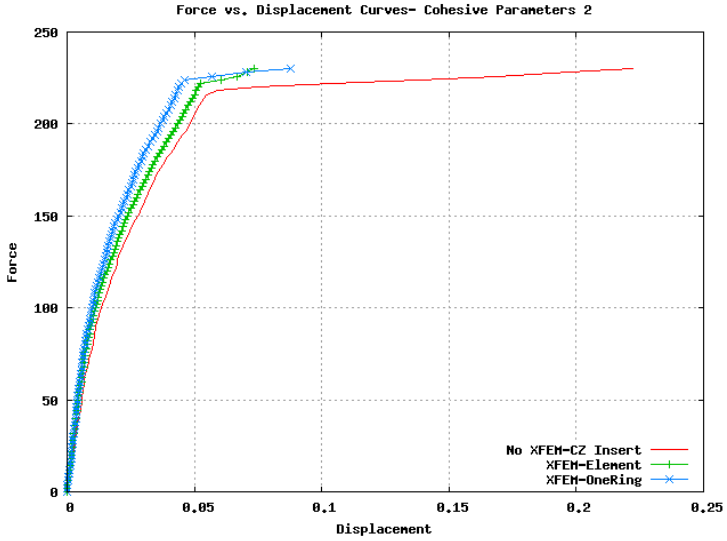

FIGURE 5.5: Force vs. displacement curve for cohesive parameters.

6

The Branching Capability

In this section, we describe the branching capability that has been implemented. The branching mechanism is heavily dependent on the duplication algorithm previously described in Chapter 3.

6.1 The Mechanics of Branching

In experimenting with the duplication algorithm, it was found that there was no clear restriction pertaining to the number of cracks within a single element. However, for implementation simplicity, branching was limited to coming from a single point on an element edge (e.g. from a virtual node on the element edge created by the first cut). In other words, an element edge can only be cut once; if the failure criterion for branching is reached for the element, but the branch would intersect an element edge that has already been cut, the crack is not allowed to branch in this element at this timestep. Examples of cases where branching can and cannot occur can be seen in Figure 6.1.

The candidate elements where branching can occur are all of the elements that have already been cut. The user-defined failure condition is examined for each element, and if the value becomes greater than the failure criteria, the stress eigenvectors are calculated and used to determine the possible branching direction. If the branching direction is a valid direction (e.g. it will not intersect an edge that has already been cut), the new cut is made.

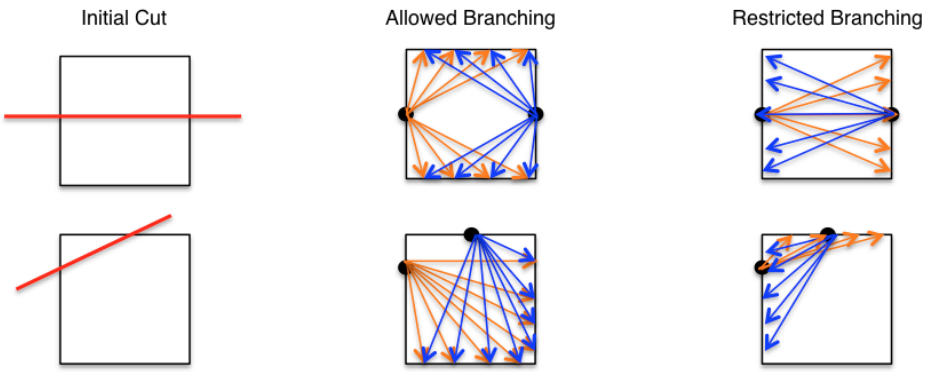

FIGURE 6.1: Examples of branching allowances and restrictions.

7

Numerical Examples for Branching

The purpose of the following numerical examples is to evaluate the implemented branching mechanism. Again, the problems solved have a known solution (either experimentally or computationally), and have some measure of comparison with other documented answers. Before delving into the problems themselves, a brief outline of the Cohesive Network Approach (the approach used for comparison) will be presented.

7.1 The Cohesive Network Approach

The Cohesive Network Approach (CNA) was presented by Xu and Needleman (1994). This approach attempts to solve fracture problems by inserting cohesive elements between every element boundary of the domain. In other words, for shell elements, every internal edge becomes a cohesive element, and for 3D elements, every internal surface becomes a cohesive element. As each element is displaced in time, the pair of internal edges moves relative to one another (corresponding to crack opening/closing/tangential movement). This separation combined with the calculated cohesive force from the cohesive law (or traction-separation law) yields the cohesive energy. When the cohesive energy is greater than the user defined energy, the cohesion gives way and a "crack" opens on the geometry. One of the major benefits to this method is that crack branching is automatically accounted for; thus, it is a good method to compare the X-FEM results to.

Currently, all CNA solutions were generated with solid hexahedral elements; this was due to the framework already in the code. Future studies include running these problems again, using the CNA for shell elements.

7.2 Plate with two holes under tensile loading

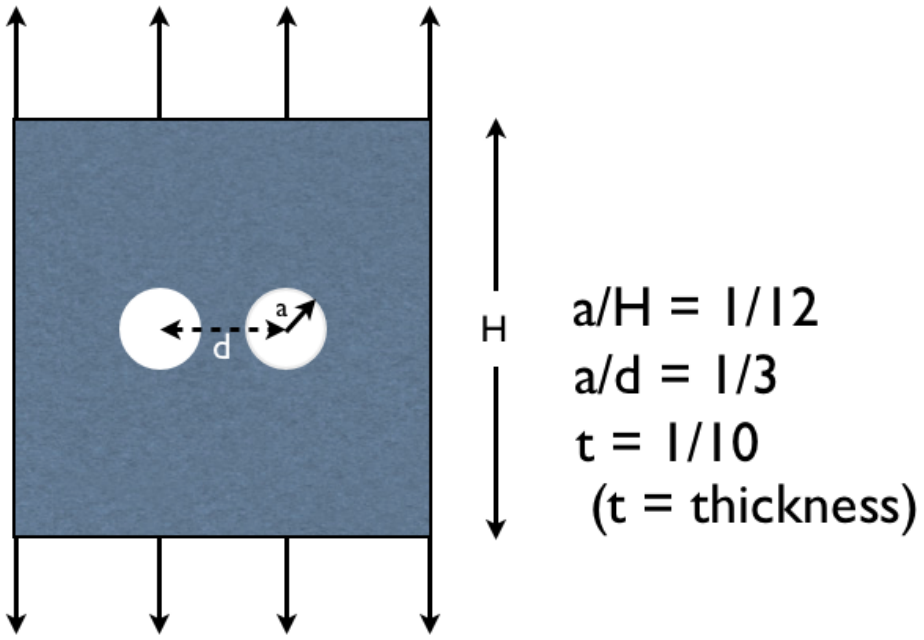

FIGURE 7.1: Plate with two holes problem setup.

Consider the problem shown in Figure 7.1 above: a plate with two holes under uniform tensile loading. Logically, as the force increases as the top and bottom are pulled apart, a stress concentration forms at the sides of each hole. Once the fracture stress of the material is reached, a crack should form connecting the two holes.

A comparative study was done for this problem, comparing the solutions found using the X-FEM nucleation and branching methods with the solutions found using the Cohesive Network Approach.

As can be seen from the stress contour plot below (Figure 7.2), the initial assessment of the problem is correct. As the plate displaces, stress concentrations arise around the holes. The holes do in fact coalesce after the fracture stress of the material is reached, and the crack continues to grow through the plate until the two halves become separated. Both the CNA as well as the X-FEM predict the two

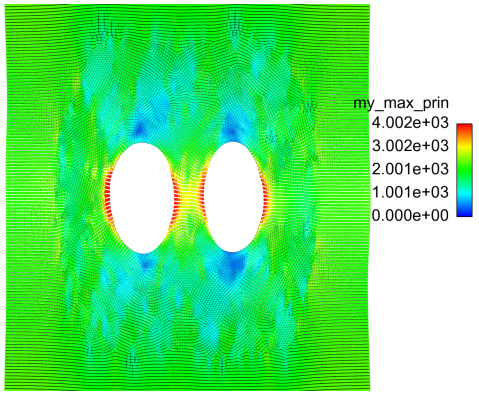

FIGURE 7.2: Plate with two holes before crack initiation.

halves separating, but give slightly different results when examined more closely.

Figure 7.3 shows a comparison of the CNA crack geometries (above) and the X-FEM crack geometries (below). Examining the pictures on the left side, it is apparent that the CNA predicts crack formation on the exterior areas of the holes before the X-FEM does. It is more logical to have cracks form on the interior areas of the holes before the exterior areas (because the interior stress concentration is higher), and thus, the X-FEM is more correct during this initial timestep. Examining the middle figures, both approaches seem to compare very reasonably. Both approaches have cracks connecting the two holes and two cracks opening on the outsides of the holes. The results on the far right still look similar, but the CNA appears to have spurious crack nucleation further away from the holes than expected. The X-FEM approach has a more correct result during this timestep as well.

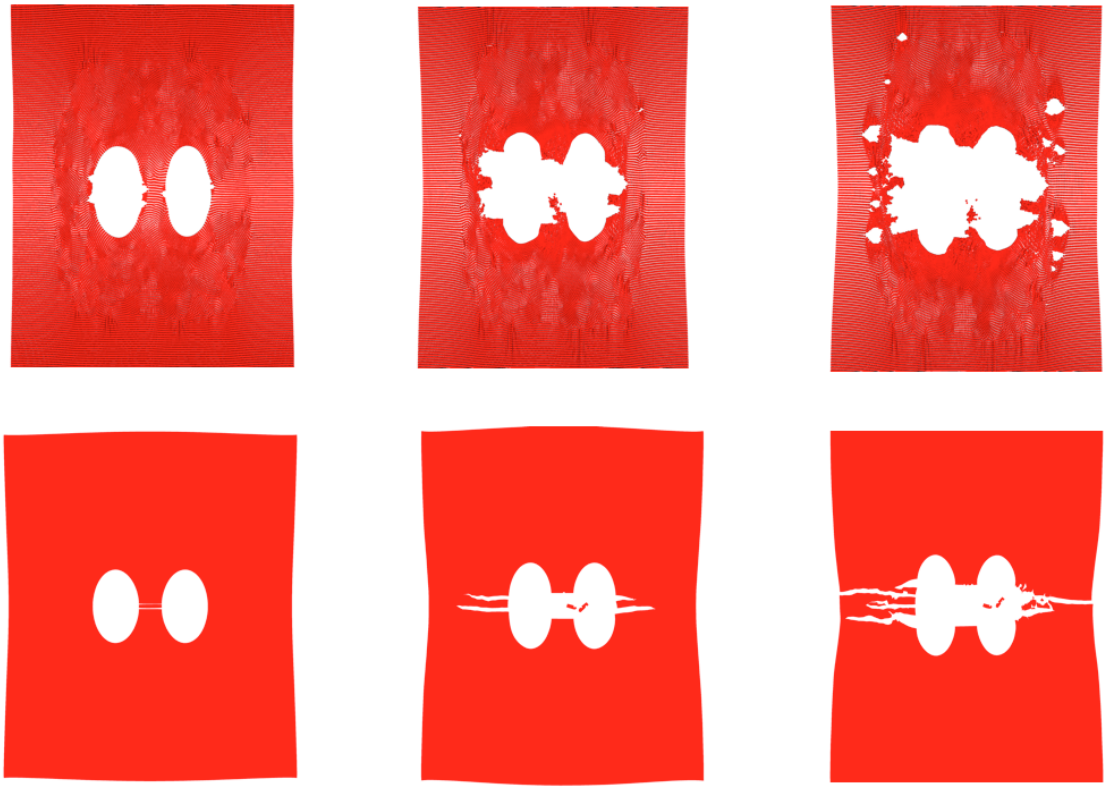

FIGURE 7.3: Plate with two holes CNA(above) vs. X-FEM(below).

7.3 Plate with Multiple Holes

Consider the problem shown in Figure 7.4 below: a plate with four holes under tensile loading at the top and bottom of the plate. For this problem, a displacement was applied at the top and bottom of the plate instead of a force. This was done in order to keep the deformation at the top and bottom consistent between the two approaches. It is understood that cracks will again nucleate around the holes as the force increases. The stress concentration will be higher at the larger holes first, then as the problem proceeds, will propagate throughout the plate.

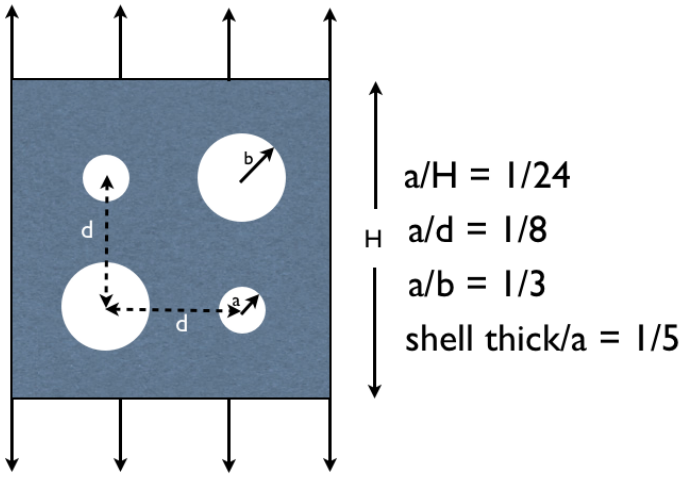

FIGURE 7.4: Plate with multiple holes problem setup

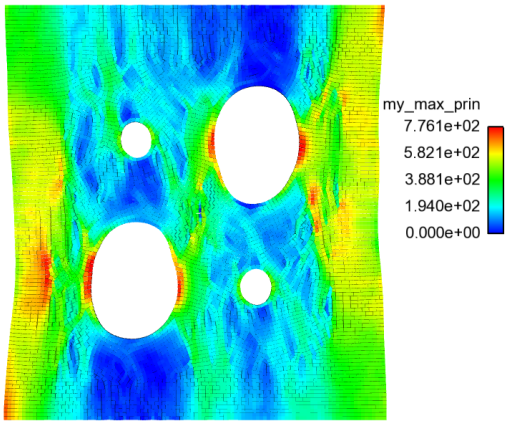

FIGURE 7.5: Plate with multiple holes before crack initiation.

As can be seen from the stress contour plot above (Figure 7.5), the stress first localizes around the large holes. In this particular case, no new cracks nucleate around the small holes, but the first cracks grow and intersect the small holes. After the small holes are intersected by the crack, the crack continues to grow through the small hole in some cases.

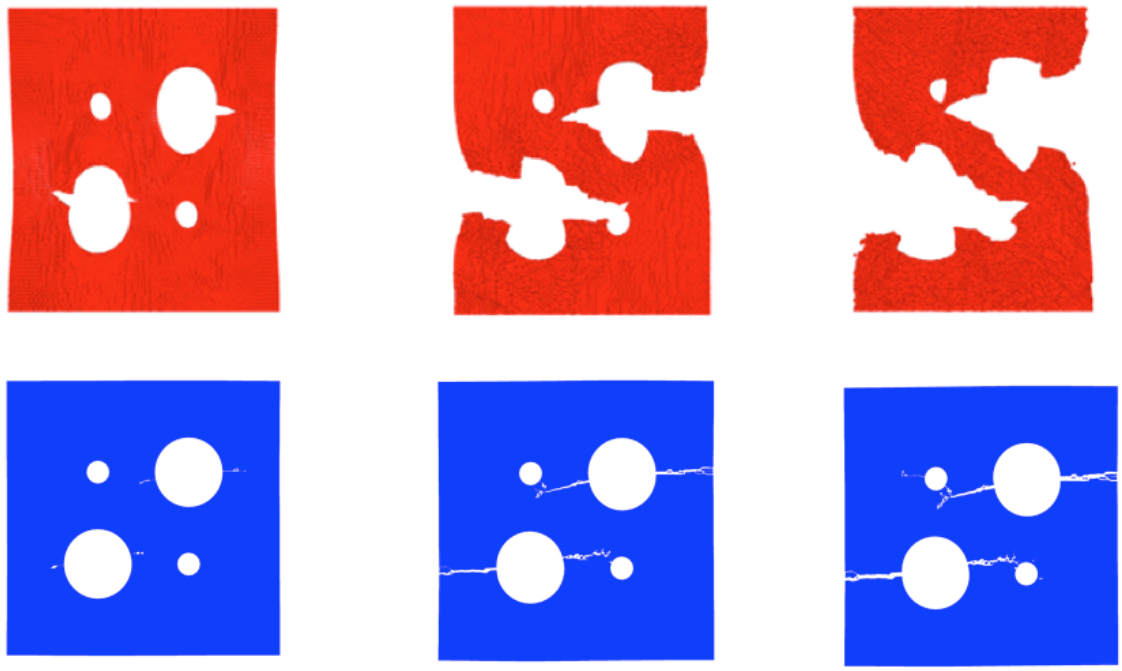

FIGURE 7.6: Plate with multiple holes CNA(above) vs. X-FEM(below).

Figure 7.6 shows a comparison of the results generated by the Cohesive Network Approach as well as by the X-FEM. Starting at the images on the left, both approaches model the first crack initiation almost exactly the same. A single crack forms on each side of the large holes when the max stress value is reached. Moving on to the images in the middle, both approaches now predict cracks coming from each side of the large holes, but the X-FEM approach predicts more growth in the top crack. This is expected because of the ability to input a growth criteria that is less than the nucleation criteria. Examining the images on the right, again the crack geometry is similar, but there are differences. In the CN simulation, the crack in the hole on the top right does not grow all the way through to the small hole on the left. In the X-FEM simulation the cracks grow all the way through and join with the small holes. Also, because of the nature of the CN approach, there is more deformation of the plate. Because of the differences in the approach of the two methods, a second

means of comparison was sought out.

7.4 The Multi-point Constraint Approach

The second approach that was examined is the multi-point constraint (MPC) approach. The MPC approach involves tying all of the elements together by their nodes via MPC's. Then, once the user defined failure criterion is reached, the MPC's give way and a crack is formed. It was believed that this approach would give closer results to the X-FEM results because the cohesive zone becomes active after the MPC's give way (thus, not interfering with the initial traction forces as the CNA does). Examining Figure 7.7 below, it does appear the MPC Approach does give results more comparable to the X-FEM results. Currently, all MPC solutions were generated with solid hexahedral elements; this was due to the framework already in the code. Future studies include running these problems again, using the MPC method for shell elements.

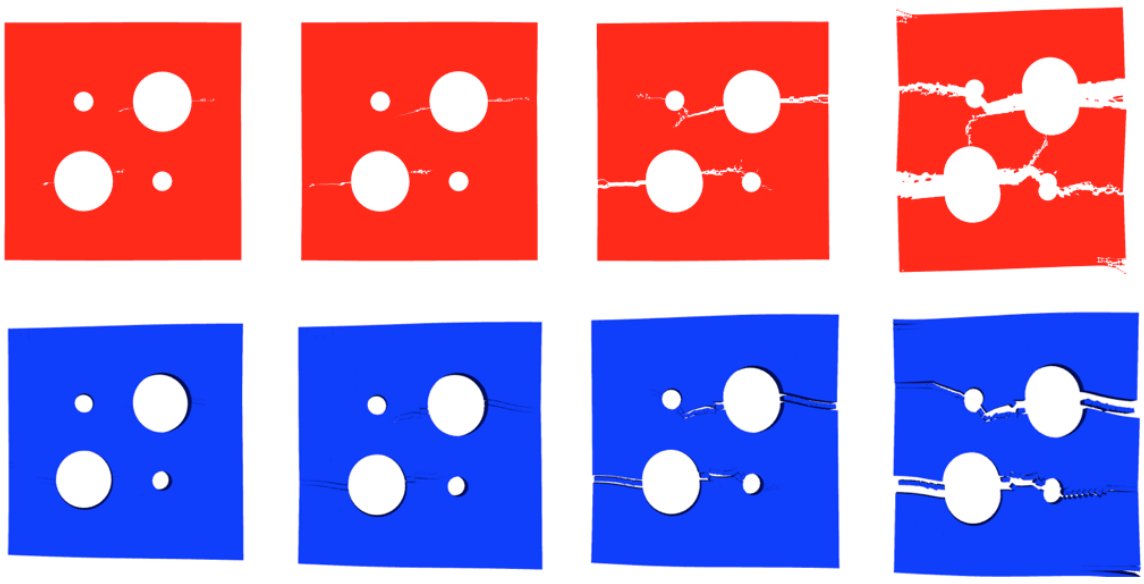

FIGURE 7.7: Plate with multiple holes MPC(above) vs. X-FEM(with CZ bottom, no CZ middle).

All four snapshots examining the X-FEM results with the MPC results compare very well. There are still slight differences between the simulations, but this is expected due to the different approaches as well as different meshes used in the MPC simulation and the X-FEM simulation. Once again, the MPC method can not specify a different growth criterion as the X-FEM method can, creating another inconsistency in the results. It is interesting to see the MPC approach generating two cracks on each side of the single hex element. It is believed that the X-FEM produces a better solution than both the CNA as well as the MPC approach because of the latter two methods requirements to fail along the element boundaries. With the X-FEM's ability to actually cut the element, this produces more accurate crack geometries.

8

Complex Numerical Simulations Coupling Nucleation and Branching

The purpose of the following numerical examples is to show the performance of the nucleation algorithm coupled with the branching algorithm on complex problems. Some of these problems may not have a known exact solution.

8.1 Pressurized Sphere

Consider the problem shown in Figure 8.1 below: a hollow sphere with an internal pressure applied within. The sphere has a slit inserted into the front (solely for the purpose of creating a stress concentration for crack nucleation), but it is not a pre-defined crack; it is simply part of the meshed geometry. As the pressure builds, the stress concentration around the slit grows until it reaches the maximum value (Figure 8.2). Then, when the value is reached, cracks form when then grow and branch into multiple cracks. The evolution of the crack patterns can be seen below in Figure 8.3.

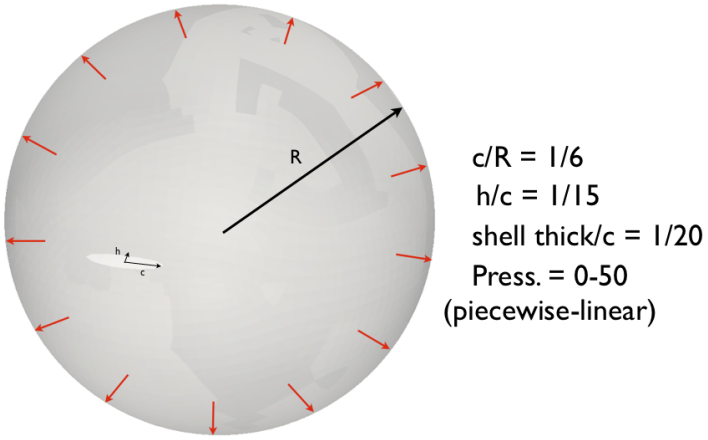

FIGURE 8.1: Pressurized sphere problem setup.

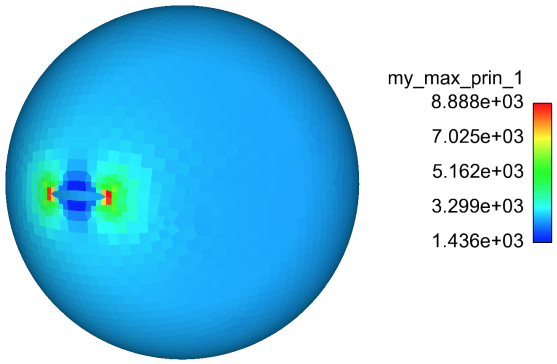

FIGURE 8.2: Pressurized sphere stress concentration.

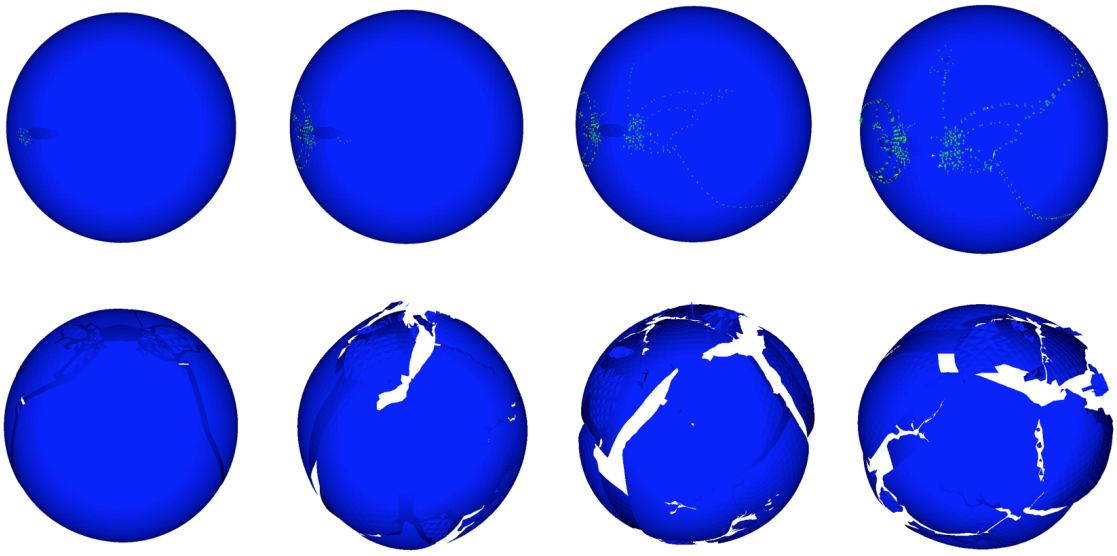

FIGURE 8.3: Crack patterns for the pressurized sphere problem.

9

Conclusion and Future Work

Although the new branching capabilities significantly increases the number of fracture problems that can be solved with the X-FEM, there still remains problems that cannot be solved using this method. One such problem is the case of a fast growing crack branching into multiple cracks, simply due to the speed by which the crack grows. If the problem is run with the current Sierra framework (and the branching capabilities turned off), one can visualize the stresses building up in the elements above and below the crack tip (Figure 9.1). Thus, the crack is wanting to branch into the V-shaped crack pattern. In the next timestep, the stress eigenvectors force the crack to turn back on itself, stopping the crack growth entirely and giving us an incorrect solution. If the problem is run with the new branching capabilities turned on, the crack still turns back on itself, but the crack branches into another crack and that crack continues to grow (Figure 9.1). This result is much more reasonable, but not as accurate as we would like. Future work involves solving this issue. Future work also involves expanding the nucleation and branching capabilities to solve 3-D problems.

New nucleation and branching algorithms have been developed for modeling complex fracture problems using the eXtended Finite Element Method. These methods have been tested and compared with other methods of solving similar problems and show great promise in the areas of accuracy, robustness, and ease of use. These methods are also attractive from the perspective of the user, in that he/she can input any element variable they desire for both nucleation and branching. These new methods for modeling dynamic fracture will hopefully act as building blocks in the computational modeling of fracture for finite elements analysis.

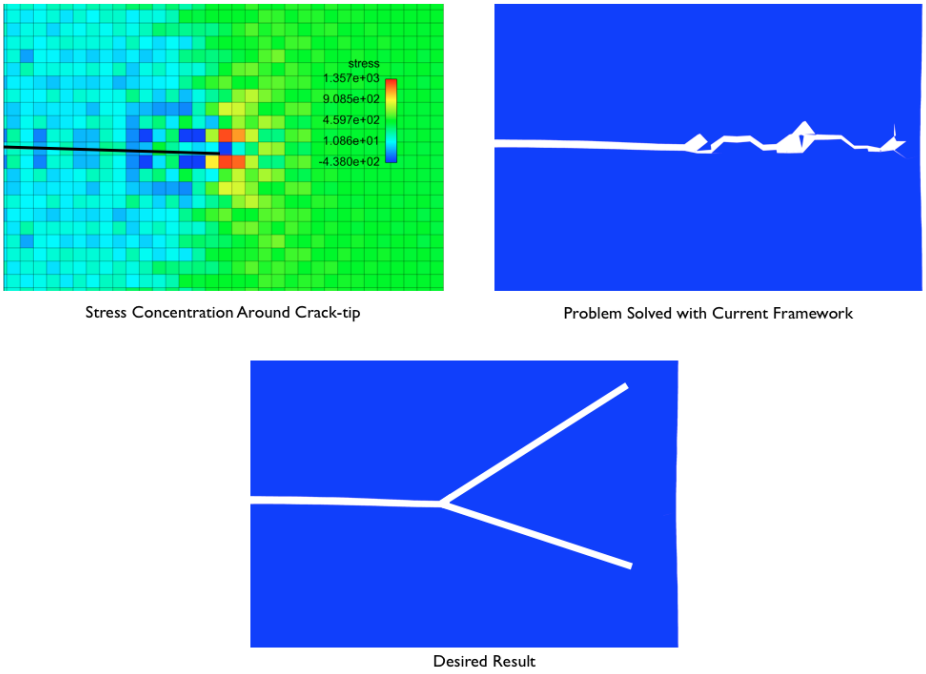

FIGURE 9.1: V-Crack branching problem.

Appendix

Appendix

A.1 Universal Material Properties

Density	0.0078
Modulus of Elasticity	210E3
Poisson's Ratio	0.3

A.2 Cohesive Properties for Plate with Hole Problem

Cohesive Properties 1

Normal Length Scale	0.01
Tangential Length Scale 1	0.03
Tangential Length Scale 2	0.03
Rotational Length Scale	0.03
Normal Energy	0.02
Tangential Energy 1	0.005
Tangential Energy 2	0.005
Rotational Energy	0.0

Cohesive Properties 2

Normal Length Scale	0.1
Tangential Length Scale 1	0.01
Tangential Length Scale 2	0.01
Rotational Length Scale	0.2
Normal Energy	1000.0
Tangential Energy 1	1000.0
Tangential Energy 2	1000.0
Rotational Energy	0.0

A.3 Cohesive Properties for Two Holes Problem

Tvergaard-Hutchinson Cohesive Properties

lambda 1	0.8
lambda 2	0.9
Normal Length Scale	0.05
Tangential Length Scale	0.1
Peak Traction	4.0E3
Failure Length Scale	0.05

Alves-Roehl Cohesive Properties

Normal Length Scale	0.01
Tangential Length Scale 1	0.03
Tangential Length Scale 2	0.03
Rotational Length Scale	0.03
Normal Energy	3.5E- 7
Tangential Energy 1	3.5E- 8
Tangential Energy 2	3.5E- 8
Rotational Energy	1.0E-10

A.4 Cohesive Properties for Multi Hole Problem

Tvergaard-Hutchinson Cohesive Properties

lambda 1	0.3
lambda 2	0.6
Normal Length Scale	0.05
Tangential Length Scale	0.1
Peak Traction	7.8E2
Failure Length Scale	0.05

Alves-Roehl Cohesive Properties

Normal Length Scale	0.04
Tangential Length Scale 1	0.06
Tangential Length Scale 2	0.06
Rotational Length Scale	0.06
Normal Energy	4E- 10
Tangential Energy 1	4.0E- 11
Tangential Energy 2	4.0E- 11
Rotational Energy	1.0E-12

A.5 Pressurized Sphere Material Properties

Density	1.0E-2
Modulus of Elasticity	1.0E7
Poisson's Ratio	0.3

Bibliography

Alves, J. L. and Roehl, D. (2012), "A New Cohesive Zone Model for Shell," *Proceedings of PACAM XII*, 12, ???–???

Belytschko, T., Chen-ShyhTsay, and Lin, J. I. (2006), "Explicit Algorithms for the Nonlinear Dynamics of Shells," *Computer Methods in Applied Mechanics and Engineering*, 195, 225–251.

Moes, N., Dolbow, J., and Belytschko, T. (1999), "Approximate Bayesian inference for latent Gaussian models by using integrated nested Laplace approximations (with discussion)," *International Journal for Numerical Methods in Engineering (UK)*, 46, 131–150.

Richardson, C. L., Hegemann, J., Sifakis, E., Hellrung, J., and Teran, J. M. (2011), "An XFEM Method for Modeling Geometrically Elaborate Crack Propagation in Brittle Materials," *International Journal for Numerical Methods in Engineering (UK)*, 88, 1042–1065.

Xu, X.-P. and Needleman, A. (1994), "Numerical Simulations of Fast Crack Growth in Brittle Solids," *Journal of Mechanics and Physical Solids*, 42, 1397–1434.